Pedestal and E_r profile evolution during an edge localized mode cycle at ASDEX Upgrade

M. Cavedon[1], T. Pütterich[1], E. Viezzer[2], F. M. Laggner[3], A. Burckhart[1], M. Dunne[1], R. Fischer[1], A. Lebschy[1,4], F. Mink[1,4], U. Stroth[1,4], M. Willensdorfer[1], E. Wolfrum[1] and the ASDEX Upgrade Team

[1]Max-Plank-Institut für Plasmaphysik, D-85748, Garching, Germany
[2] Dept. of Atomic, Molecular and Nuclear Physics, University of Seville, Avda. Reina Mercedes, 41012 Seville, Spain
[3]Institute of Applied Physics, TU Wien, Fusion@ÖAW, 1040 Vienna, Austria
[4]Physik-Department E28, Technische Universität München, 85748 Garching, Germany

18 August 2017

Abstract.

The upgrade of the edge charge exchange recombination spectroscopy diagnostic at ASDEX Upgrade (AUG) has enabled highly spatially resolved measurements of the impurity ion dynamics during an edge-localized mode cycle (ELM) with unprecedented temporal resolution, i.e. 65 µs. The increase of transport during an ELM induces a relaxation of the ion, electron edge gradients in impurity density and flows. Detailed characterization of the recovery of the edge temperature gradients reveals a difference in the ion and electron channel: the maximum ion temperature gradient ∇T_i is re-established on similar timescales as ∇n_e, which is faster than the recovery of ∇T_e. After the clamping of the maximum gradient, T_i and T_e at the pedestal top continue to rise up to the next ELM while n_e stays constant which means that the temperature pedestal and the resulting pedestal pressure widen until the next ELM. The edge radial electric field E_r at the ELM crash is found to reduce to typical L-mode values and its maximum recovers to its pre-ELM conditions on a similar time scale as for n_e and T_i. Within the uncertainties, the measurements of E_r align with their neoclassical predictions $E_{\mathrm{r,neo}}$ for most of the ELM cycle, thus indicating that E_r is dominated by collisional processes. However, between 2 and 4 ms after the ELM crash, other contributions to $\mathbf{E}\times\mathbf{B}$ flow , e.g. zonal flows or ion orbit effects, could not be excluded within the uncertainties.

1. Introduction

Since the discovery of the high confinement mode, an accompanying edge instability, called edge-localized mode (ELM), has been observed. ELMs pose one of the most serious technical challenges for future devices due to the expulsion of energy and particles onto plasma facing components within about 1 ms. Moreover, the fusion performance

projections for ITER are predicted to be bound to the pedestal characteristics [1, 2]. It is, therefore, crucial to study the evolution and recovery of the edge profiles throughout the entire ELM cycle. In particular, the dynamics of the $\mathbf{E}\times\mathbf{B}$ velocity in the edge region is of fundamental interest since its shear is believed to play an important role in the reduction of the edge turbulent transport [3].

While the recovery of the electron density (n_e) profile and the electron temperature (T_e) profile after an ELM-crash have been investigated in detail [4, 5, 6, 7], the evolution of the impurity flows and the ion temperature at the plasma edge are only poorly documented so far due to limited measurements capability. Previous studies indicate that the response to the ELM onset is a rapid increase in the temperature and $\mathbf{E}\times\mathbf{B}$ velocity in the steep gradient region followed by a drop with a longer timescale [8]. However, a comparison between the recovery of the electron and ion profiles was not performed due to the limited time resolution (550 µs) in [8]. A faster recovery of the ion temperature compared to the electron temperature was suggested in [9] but, so far, not experimentally verified. Similar studies were also performed at ASDEX Upgrade (AUG) where a collapse of the edge E_r was observed at the ELM crash [10, 11]. Here, however, the time resolution was limited to 2.3 ms. At the MAST tokamak, the dynamic evolution of the edge E_r profile during the ELM cycle was studied with a time resolution of 200 µs [12]. The edge radial electric field is observed to recover within 2 ms after the ELM crash while the electron and ion profiles could not be compared.

In this work, using the new set of edge diagnostics installed at ASDEX Upgrade (see section 2), a full characterization of the profile evolution of the edge density, temperatures, poloidal and toroidal flows with a time resolution of 65 µs is presented. The dynamics of the ions and electrons are compared and the evolution of helium as a trace impurity is investigated. Moreover, a comparison between the measured radial electric field and its neoclassical prediction during the ELM cycle is presented.

2. Experimental setup and methodology

In the last years, AUG has been equipped with several diagnostics that greatly improve the temporal and the radial resolution of measurements covering the plasma pedestal. These diagnostics as well as new analysis methods are presented following section.

2.1. Electron measurements

In the present work, the edge profiles of electron density n_e and temperature T_e have been obtained from Lithium Beam Emission Spectroscopy (Li-BES) [13, 14, 15] and the Electron Cyclotron Emission (ECE) radiometers [16], respectively. The diagnostic measurements have been combined via the integrated data analysis algorithm (IDA) [17] which, in the framework of the Bayesian theory, reconstructs the n_e and T_e profiles and their gradients with a time resolution of about 100 µs. Moreover, the ECE forward modelling developed in [18] has been employed to model the ECE emission and hence to

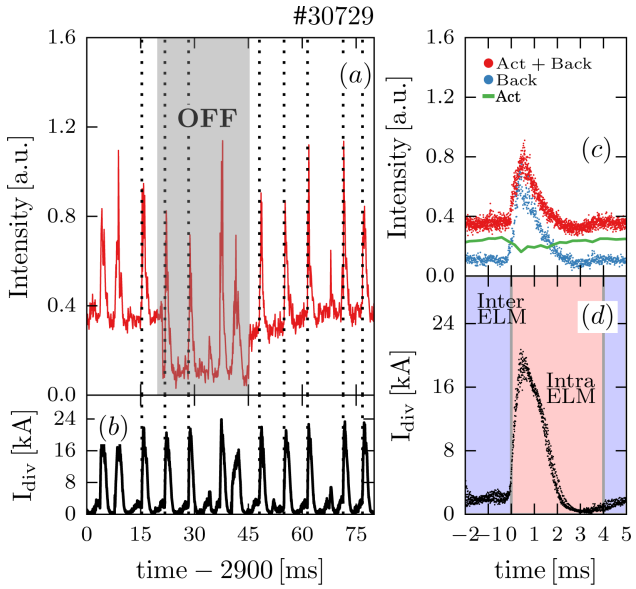

Figure 1: New method for the evaluation of intra-ELM n_e profiles based on Li-BES diagnostic: (a) evolution of the emission of one line of sight (LOS) at $\rho = 0.993$, (b) divertor shunt current I_{div}, (c) synchronized time traces of the measured signal (red) and passive (blue) and active (green) radiation, (d) synchronized time trace of I_{div}. The area highlighted in gray in figure (a) indicates the time window when the Li-beam is switched off to enable the background measurements. The inter- and intra-ELM phase are highlighted in figure (d) in blue and red, respectively.

correct for the so-called "shine-through" effect at the plasma edge [19]. This diagnostic setup was already used in the investigation of the n_e and T_e recovery after the ELM crash [7]. In this work, a new approach to determine the electron density profile from Li-BES during the ELM has been developed by consistently correcting the measured signals from the enhanced passive radiation observed during the intra-ELM phase. Figure 1a shows the measurements of one Li-BES channel during an ELMy H-mode where the gray shaded area indicates when the beam is switched off in order to measure the background radiation. The signal is compared to the divertor shunt current I_{div} (Fig. 1b) showing that both the active and passive radiation are strongly modulated by ELMs (see dashed vertical lines). To properly calculate intra-ELM density profiles, an algorithm for the background correction was developed in which the background radiation is synchronized relative to the ELM onset using I_{div} as a reference signal. This is then subtracted from the synchronized signal when the Li-beam is not switched off in order to obtain only the active part. In Figure 1c the conditional synchronized background signal (blue) and the sum of active and passive signals (red) are shown. The synchronized divertor shunt current is instead shown in figure 1d where the intra- and inter-ELM phases are highlighted in red and blue, respectively. This analysis is applied to every line of sight (LOS) and hence intra-ELM density profiles can be obtained through the IDA forward model. Note that the intra-ELM electron density measurements are also possible with

high-frequency chopping [20], however, this mode of operation is not available anymore.

2.2. Ion and flow measurements

In fusion plasmas, the ion temperature, the plasma poloidal and toroidal flows are typically measured via charge exchange recombination spectroscopy (CXRS). The ASDEX Upgrade tokamak is equipped with several CXRS systems which cover the plasma, from the low to the high field side [21, 22, 23]. A recent upgrade of the edge CXRS diagnostic provides a full reconstruction of the impurity poloidal and toroidal flows, density, temperature, and hence E_r profiles at a minimum time resolution of 10 µs [24]. Note that E_r is calculated from the radial force balance equation (RFB) $E_r = \nabla_r(n_\alpha T_\alpha)/(eZ_\alpha n_\alpha) + v_{\phi,\alpha}B_\theta - v_{\theta,\alpha}B_\phi$ by measuring every term for a specific plasma species α, in this work helium ions. While the $\mathbf{E}\times\mathbf{B}$ velocity is a property of the plasma, the single contributions in the RFB equation are different for every α and hence, for example, the poloidal and toroidal velocity of the main ions differ from the helium ones (more details con be found in [25]). High frequency measurements of E_r can also be obtained via Doppler reflectometry. However, these measurements are often not possible in H-mode because the signal to noise ratio is low due to the low turbulence level at the edge. In the cases discussed here, the $He^{2+}(n = 4 \rightarrow 3)$ transition at 468.571 nm is used for which nine LOS can be measured simultaneously. Five are used for measuring the poloidal projection of the He^{2+} velocity and four for the toroidal one. Conventional line fitting of passive and active radiation provides ion temperature and flow velocity measurements from the Doppler width and Doppler shift, while the impurity density is derived from the radiance of the emission line. In this work, particular effort has been devoted to the flux surface mapping of the CXRS measurements. A pressure constrained equilibrium reconstruction coupled with the flux diffusion equation has been used to map the different channels of all diagnostics including the CXRS system every 1 ms [26], while the reconstruction of the outer mid-plane separatrix position, available every 100 µs, has been employed to correct the mapping at the appropriate time resolution. To do that, the pressure constrained equilibrium has been rigidly shifted at every measurement time point relatively to the outer mid-plane separatrix position. Note that the latter is derived from an equilibrium reconstruction based only on magnetic measurements . In this way, the CXRS profiles can be mapped also during the intra-ELM phase where the plasma is usually observed to move inward by roughly 0.5 to 1.0 cm which is more than the diagnostic radial resolution, which is between 0.3 and 0.5 cm. Note that this procedure is mostly uncertain in the time window right after the ELM crash, i.e. in this case within 2 ms after the ELM crash, where the plasma shows the strongest inward movement.

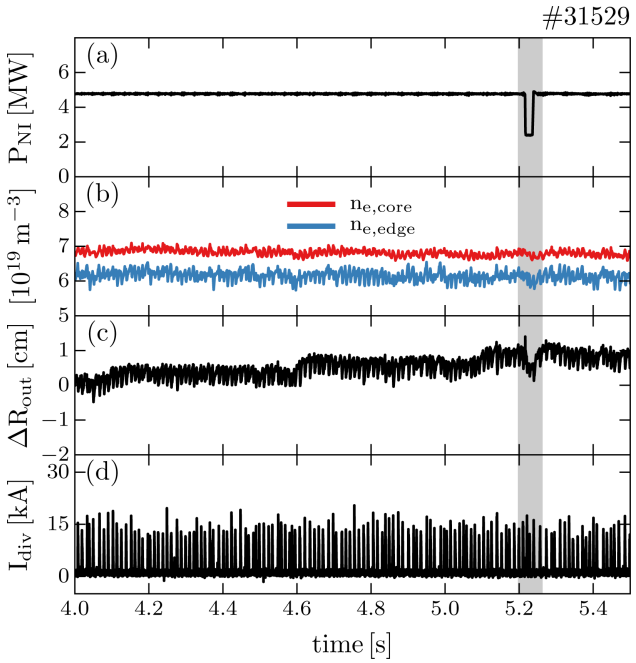

Figure 2: Timetraces of one representative discharge: (a) neutral beam input power, (b) line averaged edge (blue) and core (red) electron densities, (c) radial excursion of the plasma at the outer midplane, (d) divertor shunt current. The time window highlighted in gray has been excluded from the analysis due to the temporary drop of the heating power.

3. Edge profile evolution through-out the entire ELM-cycle

Several dedicated plasma discharges were performed to obtain high resolution measurements during the ELM cycle. In total 80 ELMs were selected to apply the analysis methods as described in Section 2 of which roughly 1/3 are used for the background measurements of the Li-BES diagnostic. The fast edge CXRS also works in a burst mode and it acquires only 2/3 of the total discharge. Hence the overall number of ELMs used in the synchronization is similar between the different diagnostics. The experiments are type-I ELMy H-mode plasmas with a toroidal magnetic field on-axis of $-2.5\,\mathrm{T}$, a plasma current of $1\,\mathrm{MA}$, a core line-averaged density of approximately $7 \times 10^{19}\,\mathrm{m}^{-3}$ and a total heating power of $8.7\,\mathrm{MW}$. Figure 2 shows time traces of the neutral beam input power (a), the line averaged density at the edge (blue) and in the core (red), the outer mid-plane plasma excursion (c) and the divertor shunt current (d). The time window highlighted in gray has been excluded from the analysis due to the temporary drop of the heating power which may affect the plasma conditions. The plasma is radially scanned through the views of the LOS to improve the radial coverage of the measurements while the other plasma parameters are kept constant. A rather constant ELM behaviour is observed in this time window with a frequency of around $85\,\mathrm{Hz}$. Note that every ELM perturbs the position of the plasma by approximately 5 to $6\,\mathrm{mm}$ (see figure 2c). This has been taken into account when mapping the CXRS

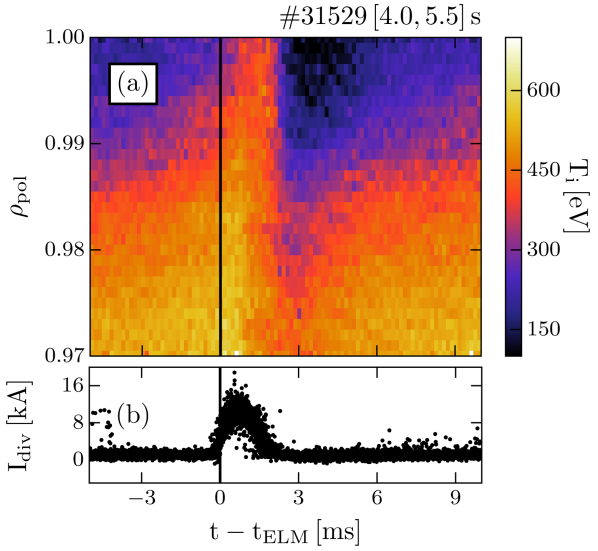

Figure 3: (a): Contour plot of the synchronized ion temperature profile as measured during an ELM cycle. (b): The divertor thermal current used as the reference signal for the synchronization.

measurements onto flux coordinates as described in Section 2.2.

The divertor shunt current I_{div} has been used as ELM monitor signal and consequently as the reference for the conditional average of the measurements. Figure 3a shows the contour plot of the synchronized ion temperature profiles where the colors indicate the measured temperatures. The synchronized reference signal, i.e. I_{div}, is shown in figure 3b. After $t - t_{\mathrm{ELM}} = 0\,\mathrm{s}$, i.e. the ELM onset, an increase of the temperature close to the separatrix is observed while the temperature at the pedestal drops. The length of this phase, usually referred to as the ELM-crash (or intra-ELM phase), is roughly 4 ms long and in general depends on the specific plasma conditions [27]. Shortly after the ELM onset, a strong reduction of T_i is observed similar to observations in DIII-D [8].

To characterize the evolution of the edge T_i, $n_{\mathrm{He}^{2+}}$ profiles and their gradients, the synchronized profiles have been fitted with a spline function. The resulting T_i and $n_{\mathrm{He}^{2+}}$ profiles from the spline fit were cross-checked with binned data showing good agreement within the uncertainties. The advantage of the spline fit in comparison with the direct 2D (time and space) binning of the data is the determination of the gradients. The splines are C^2 piecewise-polynomial functions that constrain the derivative to be continuous and derivable [28]. This is not possible if the gradients are calculated simply as differences between the binning points, which then results in an unphysical scatter. For the determination of E_r, the spline fits are only necessary when evaluating T_i and $n_{\mathrm{He}^{2+}}$, while for $v_\theta^{\mathrm{He}^{2+}}$ and $v_\phi^{\mathrm{He}^{2+}}$ standard 2D binning can be used since their gradients are not required (see radial force balance). The IDA algorithm is also based on spline functions for the reconstructed profiles thus providing the gradients automatically. This also allows for the application of 2D binning of n_e and T_e measurements and their

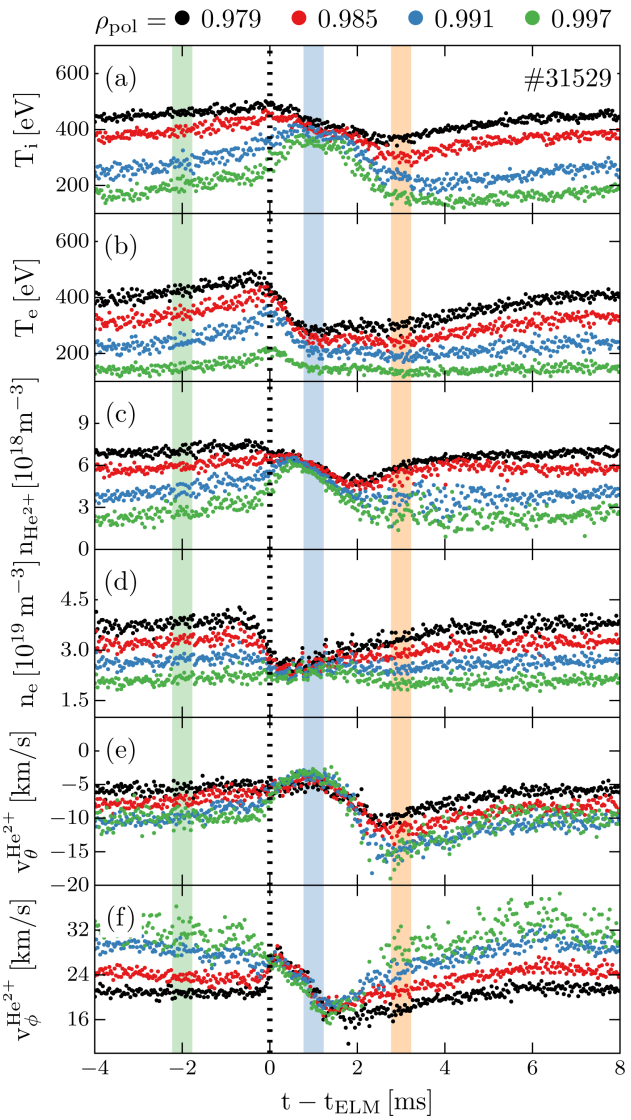

Figure 4: Evolution of the edge profiles relative to the ELM onset through the entire ELM cycle: (a) ion temperature, (b) electron temperature, (c) He^{2+} density, (d) electron density, (e) He^{2+} poloidal velocity, (f) He^{2+} toroidal velocity. The four different colors indicate the different radial positions, reported in ρ_{pol}.

gradients.

To avoid unnecessary smoothing, a time resolution of 50 µs for the binning and the fitting has been chosen, which is shorter than the acquisition time of the system, i.e. 65 µs for the CX measurements and 100 µs for the IDA algorithm. This approach was chosen in order to investigate the statistical scatter of the measurements without having to evaluate the uncertainties of the spline fits and of the profile gradients, which can not be unambiguously determined.

Figure 4 shows the evolution of the edge profiles throughout the entire ELM cycle. The profiles are reported as time-traces at four different radial locations (see colors) within the outermost 1.5 to 2 cm. The figures 4a and 4b show the ion and the electron

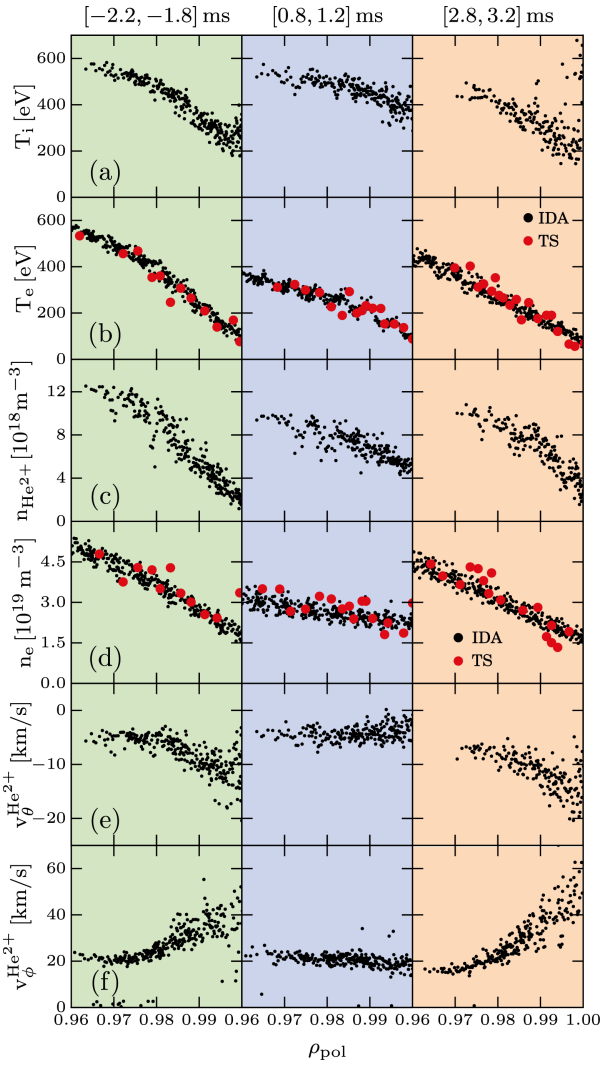

Figure 5: Edge profiles at three distinct time windows (as highlighted in figure 4) relative to the ELM onset: (a) ion temperature, (b) electron temperature from Thomson scattering (red) and from the IDA algorithm (black), (c) He^{2+} density, (d) electron density from Thomson scattering (red) and from the IDA algorithm (black), (e) He^{2+} poloidal velocity, (f) He^{2+} toroidal velocity. The three different color panels indicate the different time windows.

temperature, respectively, while in figures 4c and 4d the He^{2+} density and the electron density are presented. Additionally, the helium toroidal and poloidal flows are shown in figures 4e and 4f. The time traces are shown relative to the ELM onset defined by the rise of the divertor shunt current (see figure 3b). Note that the ELM takes place at the mid-plane and the expelled heat and particle fluxes reach the divertor few hundred of micro-seconds later. Therefore the synchronized profiles are affected from the ELM at slightly negative times. The complete edge profiles measured during the highlighted time windows are instead reported in figure 5 in which the electron density and temperature from the IDA algorithm are compared to the Thomson scattering data (fig. 5b and 5d).

The behaviour of T_i at the ELM onset is found to differ substantially from that of the electron temperature. The heat pulse originating in the steep gradient at $\rho \approx 0.98$ leaves the electron temperature close to the separatrix almost unperturbed while T_i is observed to increase (compare blue and green time traces) in agreement with the results from DIII-D [29]. This might be due to the combination of two effects: (i) the electron cyclotron emission close to the separatrix is dominated by the so called "shine through" which complicates the reconstruction of T_e profiles, (ii) in order to recover the measurements in that region a forward modelling of the ECE emission has been applied in which a two-point model forces the separatrix T_e to be close to 100 eV. This condition is based on physics assumptions of a high parallel electron heat conductivity in the SOL and thus should also hold during the ELM crash [30]. To test the hypothesis, Thomson scattering measurements have been evaluated and, within the error bars, no detectable changes of the separatrix T_e during an ELM cycle have been observed at the very edge of the plasma (see figure 5b), as reported in [29]. Further inside the plasma, towards the pedestal top region, T_i and T_e show a similar behaviour (black and red time traces in figures 4a,b). The phase of enhanced T_i nicely correlates with the detection of hot filaments (T_i up to 100 eV) during the ELM-crash [31]. The electron density during the ELM crash shown in figure 4d has been evaluated using the conditional synchronization approach described in section 2.1. The evolutions of n_e and $n_{\mathrm{He}^{2+}}$throughout the entire ELM cycle are similar: after the flattening of the gradient, the pre-ELM profiles are re-established on a shorter time scale compared to T_e, as already reported in [7]. However, during the first 2 ms after the ELM onset a stronger increase of $n_{\mathrm{He}^{2+}}$compared to n_e close to the separatrix is observed (figures 4c and 4d). This difference is probably connected to the different charges of the considered ions. A higher temperature (energy) is required to fully ionise helium compared to deuterium. Hence, the $n_{\mathrm{He}^{2+}}$profile is shifted inwards compared to the n_e profile and consequently also the pivot point during the ELM crash. Therefore a much stronger increase of the $n_{\mathrm{He}^{2+}}$profile close to the separatrix is expected. Note that a small increase of n_e at the separatrix is also observed (figure 5d) at the ELM crash which propagates outwards in the SOL indicating that the pivot point is close to the separatrix as reported in previous publications [32, 33, 20]. This is consistent with the observations in DIII-D [29] in which the pivot point of the C^{6+} density profile is observed to be further in due to the higher ionisation energy.

The behaviour of the poloidal and toroidal velocities appear more puzzling (figures 4e,f): the gradient of $v_\theta^{\mathrm{He}^{2+}}$ shows a collapse at the ELM onset similar to the other profiles but, just after it, a fast poloidal spin-up is observed and the pre-ELM profile is re-established by its slowing down. Note that these discharges were performed in deuterium with roughly 12% helium. Therefore, the behaviour of $v_\theta^{\mathrm{He}^{2+}}$ is specific only to He^{2+} as an impurity ion and is different from the main ion poloidal rotation or any other impurities. For instance, this effect has not been observed in the recovery of the N^{7+} poloidal velocity. The helium toroidal velocity represents a reversed shear moving towards the separatrix, as reported in [34]. At the ELM crash, the shear suddenly collapses to a flat profile and shortly after, the whole edge profile drops. Later, $v_\phi^{\mathrm{He}^{2+}}$

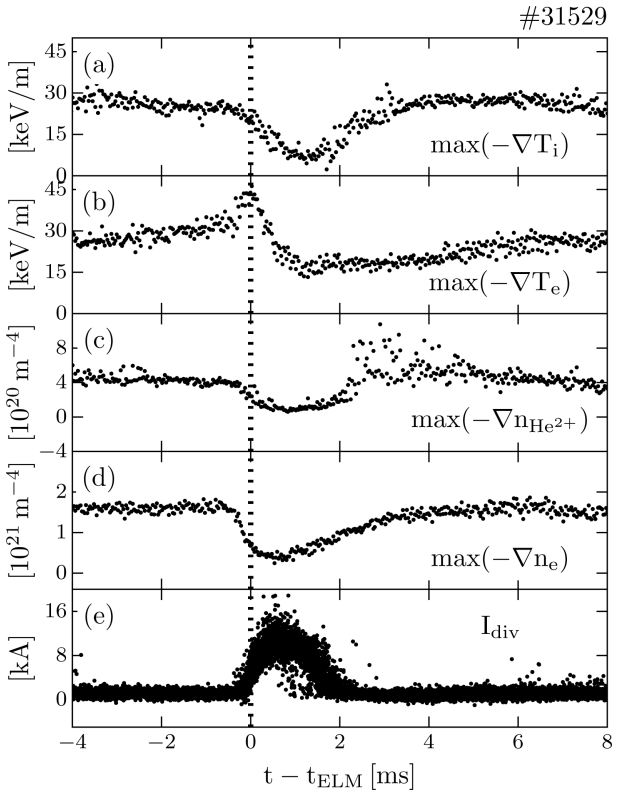

Figure 6: Evolution of the maximum edge profile gradients during an ELM cycle: (a) $\max(-\nabla T_i)$, (b) $\max(-\nabla T_e)$, (c) $\max(-\nabla n_{\mathrm{He}^{2+}})$, (d) $\max(-\nabla n_e)$. The gradients are synchronized to the increase of the divertor shunt current, shown in 3b.

recovers to the pre-ELM profile on similar timescales as the poloidal velocity. The evolution of both $v_\theta^{\mathrm{He}^{2+}}$ and $v_\phi^{\mathrm{He}^{2+}}$ is again consistent with the observations in DIII-D.

4. Behaviour of the edge temperature and density gradients

The study of the edge density and temperature gradients during the ELM cycle allows investigations of the evolution of the heat and particle transport. In particular, due to the improved capabilities of the edge CXRS diagnostics, the recovery of ∇T_i and ∇T_e can be compared at AUG for the first time.

Figure 6 shows the evolution of (a) $\max(-\nabla T_i)$, (b) $\max(-\nabla T_e)$, (c) $\max(-\nabla n_{\mathrm{He}^{2+}})$, (d) $\max(-\nabla n_e)$ during an entire ELM cycle. The time-traces are synchronized relative to the increase of the divertor shunt current (figure 6e). The ion and electron temperature gradients show different evolutions during the ELM cycle: the maximum T_e gradient recovery after the ELM crash lasts almost the entire inter-ELM period while ∇T_i is re-established on much shorter time scales, i.e. approximately 4 ms after the ELM crash. A slight decrease of $\max(-\nabla T_i)$ is also observed approaching the ELM onset. This is, however, within the error bars. As already reported in [7], the maximum of the electron density gradient is also re-established on a shorter timescale

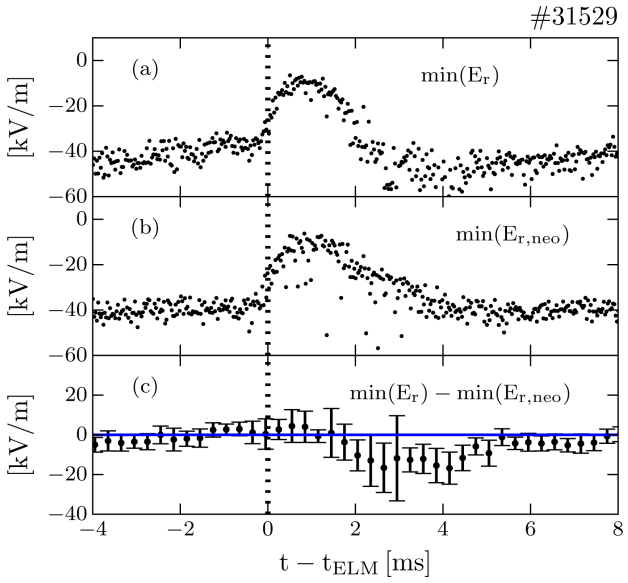

Figure 7: Comparison between the evolution of the minimum of the edge radial electric field $\min(E_r)$ (a) and its neoclassical prediction $\min(E_{\mathrm{r,neo}})$ (b) during an ELM cycle. In (c) the difference $\min(E_r) - \min(E_{\mathrm{r,neo}})$ is shown where the error bars are derived from the standard deviation of the time traces in (a) and (b) calculated every 650 µs. The time traces are synchronized relative to the onset of the divertor shunt current shown in figure 3b.

compared to ∇T_e. Within the uncertainties, ∇T_i, ∇n_e and $\nabla n_{\mathrm{He}^{2+}}$ show a similar evolution. The separation of the recovery of the ion and electron temperature gradients is consistent with observation in helium discharges [35]. After the clamping of the maximum T_i and n_e gradients, i.e. roughly 4 ms after the ELM crash, the electron density is already at the pre-ELM level (figure 4d). Instead T_i keeps increasing up to the next ELM (see figure 4a). This suggests that the pedestal becomes wider during the entire ELM cycle. At the same time, high frequency magnetic fluctuations ($\nu \approx 200{-}300$ Hz), not shown here, set in which might be responsible for the clamping of the edge gradients [36, 37]. This observation suggest that there are two different mechanisms defining the H-mode pedestal evolution during the ELM cycle as reported in [38]: one mechanisms clamps the gradient, e.g. kinetic ballooning modes [38] or microtearing modes [39]. The other mechanisms finally leads to the ELM crash, e.g. peeling ballooning modes. Further considerations on the stability of the pedestal are beyond the scope of this work and will be performed in future investigations. Stability calculation have been performed for similar discharges which were found to be close to the linear stability boundary [35].

5. The evolution of $\mathbf{E_r}$ during an ELM cycle and comparison with neoclassical predictions

The $\mathbf{E}\times\mathbf{B}$ velocity in the edge region of the H-mode is believed to shear turbulence and, hence, to sustain the edge transport barrier. Despite its importance, it has been so far poorly documented due to the complexity of the measurements. In this section, the measurements of E_r during an entire ELM are presented for the first time with the unprecedented time resolution of 65 µs. To clarify the driving mechanisms of E_r, the measurements are compared to their neoclassical approximation. Any deviation between experimental data and simulations would indicate the presence of an additional $v_{\mathrm{E}\times\mathrm{B}}$ driving mechanisms, which would add to the neoclassical (or collisional) contribution, such as turbulence driven flows [40] or ion orbit loss effects [41]. So far, these comparisons were restricted to the phase before the ELM crash due to the limited time resolution.

Figure 7 compares the evolution of the minimum of the measured radial electric field $\min(E_r)$ (a) to its neoclassical prediction $\min(E_{r,\mathrm{neo}})$ (b) during the entire ELM cycle. The neoclassical E_r has been approximated as $E_{\mathrm{r,neo}} \approx 1/(en_i)\cdot\partial p_i/\partial r$, where p_i and n_i are the main ion pressure and density, respectively, and assuming $\nabla n_e/n_e \approx \nabla n_i/n_i$. These approximations are valid given the small contribution from the toroidal velocity at the plasma edge [42] and has been tested against the NEOART neoclassical code for several individual time points [43]. The radial electric field and its associated shear show a strong collapse at the ELM onset which leads, for a short time (≤ 1 ms), to values close to typical L-mode profiles in which the minimum of the E_r well is below -15 kV/m [44]. The pre-ELM E_r profile is re-established in approximately 3–4 ms as already suggested by the evolution of T_i, $n_{\mathrm{He}^{2+}}$, $v_\theta^{\mathrm{He}^{2+}}$ and $v_\phi^{\mathrm{He}^{2+}}$ (figure 4) and consistent with previous measurements [8]. Figure 7c shows the difference $\min(E_r) - \min(E_{\mathrm{r,neo}})$ where the error bars are derived from the standard deviation of the time traces $\min(E_r)$ and $\min(E_{\mathrm{r,neo}})$ calculated every 650 µs. Within the uncertainties, the E_r and $E_{r,\mathrm{neo}}$ profiles do not show significant deviations indicating that the main ions are at rest except between 2 and 4 ms. This is consistent with earlier results from AUG [42] and Alcator C-Mod [45] where the pre-ELM E_r profile was in agreement with neoclassical prediction but in contrast to the findings from the DIII-D tokamak where additional contributions to E_r are suggested during this phase [46]. In the time window approximately between 2 and 4 ms after the ELM crash, E_r is observed to be stronger that $E_{\mathrm{r,neo}}$ indicating that additional $v_{\mathrm{E}\times\mathrm{B}}$ driving mechanisms set in during this phase and contribute to the total $\mathbf{E}\times\mathbf{B}$ flow. The deviations are, however, in the phase where the scatter of the measurements increases due to the uncertainties in the mapping and in the normalized impurity density gradient ($\nabla n_{\mathrm{He}}/n_{\mathrm{He}}$, see figure 6c). Moreover, in this particular ELM cycle phase, the assumption $\nabla n_e/n_e \approx \nabla n_i/n_i$ might not be valid. Hence, further investigations are required to confirm this observation.

6. Conclusions and Outlook

In this work the evolutions of the edge ion and electron profiles are analysed during an ELM cycle with unprecedented time resolution of 65 µs. At the ELM onset, all the edge profile gradients flatten including the impurity flow profiles of helium. In particular, the response is characterized by a rapid increase in the ion temperature and the impurity velocity in the high gradient region followed by a drop similar to previous observations at DIII-D [29]. The comparison of the dynamics between the ion and electron temperatures reveals a clearly different recovery time after the ELM onset: the maximum of the ion temperature gradient is re-established approximately 4 ms after the ELM crash, similar to the electron density temperature gradient whereas the electron temperature gradient recovery takes much longer, 7 to 8 ms. The observed separation in the evolution of the ion and electron channels confirms the hypothesis in [9] where the reconstructed edge current density has been found to deviate from the calculated one assuming $T_i = T_e$ suggesting a faster recovery of ∇T_i. The edge radial electric field is reduced to values close to typical L-mode profiles at the ELM crash and recovers to pre-ELM values within 4 ms. From this time point on, the ion temperature and the electron density gradients remain fixed while the electron temperature keeps increasing. At the same time, i.e. 4 ms, high frequency magnetic fluctuations set on which might be responsible for the clamping of the gradients [36]. Finally, the measurements and the neoclassical prediction of E_r have been compared, showing no large discrepancies within the error bars, suggesting that the edge $v_{\mathrm{E}\times\mathrm{B}}$ velocity is dominated by collisional processes for most of the ELM cycle. However, between 2 and 4 ms after the ELM onset E_r deviates from its neoclassical prediction suggesting that additional driving mechanisms could contribute to the $\mathbf{E}\times\mathbf{B}$ flow. On the other hand, during this phase the uncertainties of the measurements largely increase. Hence, to confirm this observation different types of ELMs need to be considered and possibly the main ions flows should be directly measured by investigating pure helium discharges at high time resolution. Moreover, it is foreseen to study plasmas with high triangularity in which a lower ELM frequency is usually observed. Furthermore, nitrogen seeding can be employed to study a different impurity species and to analysed different types of ELMs.

Acknowledgments

This work has been carried out within the framework of the EUROfusion Consortium and has received funding from the Euratom research and training programme 2014-2018 under grant agreement No 633053. The views and opinions expressed herein do not necessarily reflect those of the European Commission. F.M. Laggner is a fellow of the Friedrich Schiedel Foundation for Energy Technology.

References

[1] J.E. Kinsey et al. *Nucl. Fusion*, 43(12):1845, 2003.

[2] E. J. Doyle (Chair Transport Physics) et al. *Nucl. Fusion*, 47(6):S18, 2007.

[3] H. Biglari et al. *Phys. of Fluids B: Plasma Phys.*, 2(1):1, 1990.

[4] R. Behn et al. *Plasma Phys. and Contr. Fusion*, 49(8):1289, 2007.

[5] R. J. Groebner et al. *Nucl. Fusion*, 49(4):045013, 2009.

[6] M. N. A. Beurskens et al. *Nucl. Fusion*, 49(12):125006, 2009.

[7] A. Burckhart et al. *Plasma Phys. and Contr. Fusion*, 52(10):105010, 2010.

[8] M. R. Wade et al. *Phys. Rev. Lett.*, 94:225001, 22, 2005.

[9] M. G. Dunne et al. *Nucl. Fusion*, 52(12):123014, 2012.

[10] E. Viezzer et al. *Nucl. Fusion*, 53(5):053005, 2013.

[11] T. Pütterich et al. *J. Nucl. Mater.*, 415(1, Supplement):S334–S339, 2011. Proceedings of the 19th International Conference on Plasma-Surface Interactions in Controlled Fusion.

[12] H. Meyer et al. *Nucl. Fusion*, 51(11):113011, 2011.

[13] J. Schweinzer et al. *Plasma Phys. and Contr. Fusion*, 34(7):1173, 1992.

[14] R. Fischer et al. *Plasma Phys. and Contr. Fusion*, 50(8):085009, 2008.

[15] M. Willensdorfer et al. *Plasma Phys. and Contr. Fusion*, 56(2):025008, 2014.

[16] N. A. Salmon. *Int. J. Infrared Milli.*, 15(1):53–60, 1994.

[17] R. Fischer et al. *Fusion Sci. Technol.*, 58(2):675–684, 2010.

[18] S. K. Rathgeber et al. *Plasma Phys. and Contr. Fusion*, 55(2):025004, 2013.

[19] E. de la Luna et al. *Rev. Sci. Instrum.*, 75(10):3831–3833, 2004.

[20] M. Willensdorfer et al. *Rev. Sci. Instrum.*, 83(2), 023501, 2012.

[21] E. Viezzer et al. *Rev. Sci. Instrum.*, 83(10), 103501, 2012.

[22] A. Lebschy et al. In *42nd EPS Conference on Plasma Physics*, 2015.

[23] R. M. McDermott et al. *accepted for publication*, 2017.

[24] M. Cavedon et al. *Review of Scientific Instruments*, 88(4):043103, 2017.

[25] K. Ida. *Plasma Physics and Controlled Fusion*, 40(8):1429, 1998.

[26] R. Fischer et al. *Fusion Sci. Technol.*, 69(2), 2016.

[27] P. A. Schneider et al. *Plasma Phys. and Contr. Fusion*, 56(2):025011, 2014.

[28] C. De Boor, number Bd. 27 in Applied Mathematical Sciences. Springer-Verlag, 1978.

[29] M. R. Wade et al. *Phys. Plasmas*, 12(5):056120, 2005.

[30] J. Neuhauser et al. *Plasma Phys. and Contr. Fusion*, 44(6):855, 2002.

[31] M. Kočan et al. *Contributions to Plasma Physics*, 53(1):22–26, 2013.

[32] S. Soldatov et al. In *Proceedings of the 36th EPS Conference on Plasma Physics, Sofia, Bulgaria.* 2009.

[33] I. Nunes et al. *Nuclear Fusion*, 45(12):1550, 2005.

[34] T. Pütterich et al. *Phys. Rev. Lett.*, 102:025001, 2, 2009.

[35] F. M. Laggner et al. *Physics of Plasmas*, 24(5):056105, 2017.

[36] F. M. Laggner et al. *Plasma Phys. and Contr. Fusion*, 58(6):065005, 2016.

[37] F. Mink et al. *Plasma Phys. and Contr. Fusion*, 58(12):125013, 2016.

[38] P.B. Snyder et al. *Nuclear Fusion*, 51(10):103016, 2011.

[39] D.R. Hatch et al. *Nuclear Fusion*, 55(6):063028, 2015.

[40] P H Diamond et al. *Plasma Phys. and Contr. Fusion*, 47(5):R35, 2005.

[41] K. C. Shaing et al. *Phys. Rev. Lett.*, 63:2369–2372, 21, 1989.

[42] E. Viezzer et al. *Nucl. Fusion*, 54(1):012003, 2014.

[43] A. G. Peeters. *Phys. Plasmas*, 7(1):268–275, 2000.

[44] P. Sauter et al. *Nucl. Fusion*, 52(1):012001, January 2012.

[45] R. M. McDermott et al. *Phys. Plasmas*, 16(5), 056103, 2009.

[46] J. Kim et al. *Phys. Rev. Lett.*, 72:2199–2202, 14, 1994.